Active Galactic Nuclei and their role in galaxy evolution in the early universe

Derek Attewell

Master of Science

Department Physics and Astronomy

McGill University Montreal,Quebec 2014-03-01

Date222

©Derek Attewell 2014

ACKNOWLEDGEMENTS

I would like to thank my supervisor, Tracy Webb for her support and patience over the past three years. In addition, Ashley Faloon provided continuous help and guidance, helping me navigate the intricate maze that is a multi-wavelength astronomical data set. I would also like to thank Renbin Yan for his spectroscopic contributions. I would not be where I am without the love and support (in many ways) of my parents, and want to thank them for always trusting in my decisions. And finally I want to thank Tieghan Killackey for her love and surprising patience, and for believing one day I would finish this.

ABSTRACT

Galaxy evolution continues to be one of the most active and exciting areas in observational cosmology today. The fundamental mechanisms responsible for transforming the early homogeneous universe into the spectrum of complex structure we see in the local universe remain poorly understood. Active Galactic Nuclei (AGN) are black holes residing in the center of their host galaxy, actively accreting dust and gas. It is suspected that AGN play an important role in galaxy evolution through feedback and the quenching of star formation. From our sample of $\approx 50,000$ spectroscopic sources, we were successful in measuring the equivalent widths of the O[lll] and H β emission lines for 1226 sources with $\sigma > 4$, and subsequently calculating the indicative line ratio between the two. Utilizing Juneau et al. (2011)'s novel Mass Excitation Diagnostic tool, replacing the [NII]/H α line ratio with the comparable stellar mass, we identified 371 active galactic nuclei, comprising 30% of our subsample. Unfortunately we were not able to identify any observable differences between the active population and the remaining star forming galaxies, in both redshift distribution and colour-magnitude space. However we did find that all galaxies, regardless of the ionizing source occupied the blue cloud on the colour-magnitude diagram. Since our quality criteria preferentially selected sources with particularly strong O[lll] emission lines, which are known to have young stellar populations (Kauffmann et al., 2003), we therefore have identified a population of young galaxies that have luminous active nuclei residing at their center.

ABRÉGÉ

L'volution des galaxies continue d'tre l'un des sujets les plus actifs et fascinant de la cosmologie observationelle. Les meanismes fondamentaux responsables de la transformation de l'Univers jeune et homogne en un spectre de structures complexes que l'on observe aujourd'hui n'est toujours pas entirement compris. Les noyaux actifs de galaxies (AGN, pour Active Galactic Nuclei, en anglais) sont des trous noirs preent au centre de leur galaxie hte, et qui accretent poussires et gaz. On pense que ces AGN jouent un rle important dans l'volution des galaxies par rtrocontrle et touffement de la formation stellaire. Pour notre chantillon de $\approx 50,000$ sources spectroscopiques, nous avons mesur les largeurs quivalentes de raies d'missions de O[lll] et H β pour 1226 sources avec une signifiance de $\sigma > 4$. Nous avons ensuite calcul les rapports entre ces deux raies d'mission. En utilisant l'outil novateur de diagnostique d'excitation de mass de Juneau et al. (2011), et en remplaant le rapport $[NII]/H\alpha$ par la masse stellaire comparable, nous avons identifi 371 AGNs, soit 30% de notre sous-chantillon. Cependant, nous n'avons pas identifi de diffrences observationelles entre la population active et le reste des galaxies formation stellaire, et ce, dans l'espace de dealage vers le rouge et dans l'espace couleur-magnitude. Par contre, nous avons dmontr que toutes les galaxies, quelque soit la source ionisante, occupent la partie bleu du diagramme de couleur-magnitude. Puisque le critre de qualit slectionne prfrentiellement les sources avec une raie d'mission O[lll] particulirement forte, qui sont connues pour avec une population stellaire jeune (Kauffmann et al., 2003), nous avons par consquent identifi une population de galaxies jeunes possdant un noyau actif lumineux en leur centre.

TABLE OF CONTENTS

ACK	NOWI	LEDGEMENTS
ABS'	TRAC'	Γ
ABR	ÉGÉ	
LIST	OF F	IGURES
1	Introd	uction
	1.1 1.2	Hierarchical Structure Formation
	1.3	1.2.2 Red Elliptical Galaxies14Active Galactic Nuclei151.3.1 Unified Model of AGN17
	1.4	1.3.2 AGN Diagnostics20Mass Excitation Diagnostic22
2	Data	
	2.1	Photometric Observations
	2.2	Spectroscopic Data </td
	2.3	Sample Selection
3	Metho	$ds \dots \dots$
	3.1	Emission Line Measurement 37 3.1.1 Equivalent Width 38 3.1.2 Line Fitting 39 3.1.3 Signal-to-Noise 41

	3.2	Stellar Masses
4	Resul	ts
	4.1 4.2 4.3	Mass Excitation Diagnostic and AGN Identification45Redshift Distribution47Colour Evolution48
5	Concl	usion
	5.1	Future Work575.1.1 Sample Selection and Design575.1.2 Environmental Analysis595.1.3 Stellar Masses595.1.4 Conclusion59

LIST OF FIGURES

Figure		page
1–1	$AGN\ Unification\ model\ -\ http://ned.ipac.caltech.edu/level5/March12/Middelberg/Middelberg3.html\ .\ .\ .\ .\ .\ .\ .\ .\ .\ .\ .\ .\ .\$	19
1–2	Comparison between the classic BPT diagnostic diagram and the newly developed Mass Excitation diagram. In panels c) and d) we can see good agreement between where the BPT (a) populations fall on the MEx parameter space. This is in part explained by the mass-metallicty relation show in panel b). (Juneau et al., 2011)	24
1–3	Completeness and contamination rates in bins of stellar mass. (Juneau et al., 2011). (a) shows the completeness of galaxies classified as AGN using the MEx diagram and (b) shows the completeness of galaxies classified as star forming	28
1–4	Probability of a galaxy being powered by star formation or an active nucleus on the MEx diagnostic. (Juneau et al., 2011). Red lines are the dividing lines separating MEx classified AGN, SF and composite galaxies. Blue contours are areas of equal probability	29
3–1	The equivalent width of an emission line if the width of a box with the same area as the integrated flux of the emission line, and is used to measure the strength of an emission line (Mo et al., 2010).	38
3-2	Emission line fit for two examples of spectra. The first two are from a high quality spectra, where you can clearly see the guassian function fit over the emission line as well as the continuum fit. The second two are from a spectra with significant noise, which did not pass the quality cut	44

4-1	The Mass Excitation Diagnostic tool. With the $f([OIII]\lambda 5007)/f(H\beta)$ line ratio on the y-axis and M_{\star} on the x-axis, Juneau et al. (2011) define three distinct regions identifying galaxies with active nuclei (top right), star forming (bottom left) and composites (middle). Our sample exhibits suspiciously low stellar masses, discussed below.	53
4-2	Redshift distribution of the three different populations identified by the MEx diagnostic. In descending order the distributions are are: all galaxies, star forming, AGN, and barely seen are the composites. A difference in redshift is not seen here.	54
4-3	Comparison of the three different populations, as a percent of the entire sample population in redshift bins of $z=0.05$. This further emphasizes that there is no significant trends over redshift space as each population remains relatively unchanged	55
4-4	Colour vs Magnitude diagram. R-z' colour is on the y-axis with z' magnitude on the x-axis. MEx AGN are in red, MEx SF are in blue, and all spectroscopic sources (≈ 50,000) are shown in grey. We can see that both the AGN and SF galaxies both occupy the "blue cloud". Furthermore we do not see any evident significant differences between the two populations.	56
	differences between the two populations	90

CHAPTER 1 Introduction

One of the most intriguing and fundamental questions in the field of cosmology continues to be the processes and mechanisms that transformed the early homogeneous universe into the myriad of structure we observe today. Within the dominant theory of hierarchical structure formation, primordial fluctuations in the early universe provided the seeds for early galaxies, which then grew through mergers and accretion of smaller galaxies to form groups, clusters, and eventually the large scale structure we see in the local universe today (Gamow & Teller, 1939; Lifshitz, 1946; Arag et al., 1998). Although this paradigm has proven robust in recent years, its simplicity still fails to explain the wide variety of galaxy populations and morphologies we see in the universe. A more thorough understanding of the physical processes that govern the growth and evolution of galaxies, on a variety of scales and environments, is required to complete the picture of structure formation.

The Red Sequence Cluster Survey (RCS1) is an extensive survey of galaxy clusters designed to study galaxy evolution in dense environments. Up until this point it has been very difficult to identify the primary ionizing source, either active galactic nuclei (AGN) or star formation, in luminous galaxies at high redshifts due to observational limitations. This is a crucial step in understanding the fundamental processes involved in the evolution of galaxies, and yet is often disregarded because of the

lack of necessary information. With spectroscopic and photometric coverage of the RCS1, we have the exciting opportunity to classify galaxies within the RCS1 in this way, thanks to the promising and novel technique introduced by Juneau et al. (2011).

1.1 Hierarchical Structure Formation

Shortly after the big bang the universe consisted of a incredibly hot, dense plasma containing enough energy to prevent even elementary particles from forming. It was in this dense primordial plasma that initial quantum fluctuations existed as minute overdensities in the otherwise homogeneous state (Hawking, 1982). These minuscule fluctuations are believed to have been amplified during inflation to become the seeds of large scale structure observed today (Harrison, 1970; Zeldovich, 1972).

As the universe continued to cool after inflation, the temperature dropped below that of the binding energy of a nucleus, and eventually an atom, allowing hydrogen and subsequently helium to form (Abel et al., 1997). At the same time, photons were now able to travel freely through the universe due to the sudden lack of ionized plasma to interact with, during an epoch named *recombination*. These photons are the cosmic microwave background (CMB) which we observe isotropically in the night sky, and were emitted when photons decoupled from matter (Jones & Wyse, 1985).

The CMB is one of the most important and revealing tools when it comes to studying the early universe. It was emitted shortly after the big bang and is intrinsically the farthest back in time we can physically observe. Before recombination photons were trapped due to the density of protons in the primordial plasma, only travelling a minute distance before once again interacting with an ion and being re-emitted (Jones & Wyse, 1985). This had two consequences; to maintain a homogeneous temperature across the plasma, as well as trapping the photons within making the universe opaque. Therefore we can not look beyond the epoch of recombination when the CMB was emitted, making it our best glimpse into the condition of the early universe (Mo et al., 2010).

Luckily the CMB has the signature of these early conditions imprinted within it, making it an invaluable tool. One characteristic of the CMB is its remarkable homogeneity. The CMB energy spectrum matches that of a thermal black-body with a temperature of 2.72548 ± 0.00057 K (Fixsen, 2009). Yet when observed more closely the spectral radiance across angular scales show anisotropies which point to the very quantum fluctuations mentioned above (Smoot & Bennett, 1992). These are signatures one would expect to see if a uniform hot gas expanded to the size of our universe. It is the evidence of these minute overdensities which is the foundation for the hierarchical formation of large scale structure in the universe.

After recombination and the decoupling of photons, the universe entered a dark age where gravity began to dominate. First, dark matter began to collapse on to the small overdensities which originated from quantum fluctuations in the early universe (White & Rees, 1978; Arag et al., 1998). Although small, the gravitational potentials due to these overdensities were the beginning of structure in our universe (Press & Schechter, 1974; Efstathiou & Silk, 1983). During this time structure grew linearly, as dark matter only interacts through gravity. Slowly halos of dark matter began to form, eventually attracting baryonic matter as well and providing the sites for the first stars to ignite (White & Rees, 1978). Cold hydrogen and helium gas gravitationally collapsed increasing the pressure and temperature until the first star was born (Mo et al., 2010).

These stars continued to interact with neighbouring stars, eventually becoming gravitationally bound together and forming the first galaxies. Through this process of bottom-up structure formation gravity built the vast structure we see today. Galaxies continued to form and evolve through minor interactions with smaller galaxies or major mergers with systems of similar size (Press & Schechter, 1974; Mo et al., 2010). Eventually, whole systems of galaxies became gravitationally bound into small groups, clusters, super-clusters and filaments. In this way, small objects formed first and continuously evolved through interactions and mergers, forming the structure we observe in the universe today.

When studying this evolution observationally the primary goal is to explain the wide variety of galaxies we see in the night sky. Under the framework of hierarchical structure formation, a galaxy will undergo countless mergers and interactions

throughout its lifetime. It is within these interactions that we can seek answers to the question of how we can end up with such a diverse array of galaxies from such uniform beginnings.

1.2 Galaxy Populations

Before continuing it is useful to outline some general classifications of galaxy populations that will be referenced to throughout this study. These are very broad classifications and are not meant to be definitive. Rather they categorize the wide variety of observed galaxies into manageable sub-samples that share similar characteristics. From these we can begin to compare properties and hopefully draw some conclusions about the origins of each.

1.2.1 Blue Spiral Galaxies

Young gas-rich galaxies are often found in the low density field, or on the outskirts of groups and clusters. Morphologically they are most often spiral galaxies and typically are undergoing star formation creating UV light and a characteristic blue appearance. With a wealth of cold gas and dust these young galaxies often have very active star formation.

Galaxies that are undergoing an exceptionally high rate of star formation are often referred to as *starburst galaxies*. Starburst galaxies can be extremely luminous, most often in the infrared (IR), making them important tools for studying galaxy evolution in the distant universe. Galaxies in the midst of a starburst often have tidal

features or other indications of recent or ongoing interactions with nearby galaxies. These minor mergers and interactions are proposed as a mechanism for triggering starbursts by funnelling cold gas into the center of the galaxy, igniting violent star formation (Larson & Tinsley, 1978).

1.2.2 Red Elliptical Galaxies

On the other hand, massive evolved elliptical galaxies display very different characteristics. They are most often found in dense environments such as groups and clusters, dominating the center region of the cluster. Sometimes described as "red and dead", large ellipticals typically have very little cold gas remaining and hence very little star formation.

In the paradigm of hierarchical structure formation, ellipticals may have formed through multiple mergers of smaller spiral galaxies, both disrupting the tidy planar morphology as well as spurring a starburst which could quickly exhaust the cold gas quenching further star formation (Toomre & Toomre, 1972; Larson & Tinsley, 1978; White & Rees, 1978). For some of the most massive ellipticals, this process can happen many times as it resides in the bottom of the cluster potential, slowly accreting smaller galaxies.

Once again I want to reiterate these classifications are very broad and of course have plenty of overlap, as well as exceptions which can fall into both or neither. We will run into many other categories of galaxies throughout this study, yet these are two important phases evolutionarily and worth keeping in mind.

1.3 Active Galactic Nuclei

Some of the most intriguing and observationally invaluable objects in the night sky are those that are brightest. For one, such objects are observable far into the distant universe allowing us to study trends on cosmic time scales. Yet a notable luminosity is often also a symptom of an important evolutionary phase in a galaxy's life cycle. The observational challenge lies in understanding the origin of the excess luminosity. As mentioned above, starbursts can cause a galaxy to shine brightly, while some of the most luminous objects in the universe are quasars which can outshine their entire host galaxy. Therefore a complete understanding of galaxy evolution requires the study of both a galaxy's stellar population and nuclear activity, and how the two are interconnected.

It is now widely accepted that the majority of galaxies host a supermassive black hole (SMBH). It has been shown that the masses of the SMBH correlate tightly with the stellar velocity dispersion of the host bulge, suggesting a relation between the formation and evolution of massive galaxies and their central black holes (Magorrian & Tremaine, 1998).

Furthermore, the accretion history of central supermassive black holes follow a similar trend as the cosmic star formation history (Barger & Cowie, 2001). These observations suggests a fundamental connection between the central SMBH and the

star formation of a galaxy (Juneau et al., 2011). For example, radiative feedback from active black holes has been implemented in galaxy evolution simulations as a method for quenching star formation. While observational evidence exists to support the evolutionary importance of nuclear black holes, the full extent of the interplay between a black hole and the host galaxy remains unclear.

A galaxy is classified as "active" if the black hole residing in the center is currently accreting matter and therefore emitting significant amounts of radiation. It is proposed that active galactic nuclei (AGN) are an important evolutionary stage in a galaxy's life-cycle, and subsequently have received a lot of attention in recent decades (Juneau & Dickinson, 2013). Yet while there are many different diagnostic techniques for AGN, each has limitations. For example, AGN have most frequently been identified and studied using high energy X-ray emissions. However, heavily absorbed systems or low luminosity AGN are not visible in X-ray surveys. These heavily absorbed systems were first identified by the unresolved portion of the cosmic x-ray background, in conjunction with compton-thick systems in the nearby universe. Therefore it has become apparent that multi-wavelength methods are needed to study AGN in a comprehensive way.

The wide variety of AGN observed early on lead to a plethora of classifications and populations of active galaxies, from Seyferts (I and II) to Quasars to Blazars and so on. Skipping the history lesson on nomenclature, it will suffice to jump to the conclusion arrived at, termed the unification of AGN. This unified model proposed

that the large range of characteristics observed in active galaxies is a result of the asymmetry of the AGN geometry combined with the viewing angle of the observer, rather than being tracers of intrinsically distinct populations.

1.3.1 Unified Model of AGN

AGN terminology is often confusing due to classifications often reflecting historical differences, rather than physical distinctions. The plethora of categories that resulted are not directly applicable to work here, yet it is important to understand the current unified model of AGN before moving forward.

One major difference observed in early AGN was the presence, or lack of, Broad Line Regions (BLR). Spectral emission lines are a typical indicator of nuclear activity in a galaxy (Orr & Browne, 1982). Molecules in the interstellar medium (ISM) are excited by nuclear emission and then produce characteristic lines. The radiation is emitted at a specific discrete wavelength creating the observable emission line, on top of the continuum. However if the gas creating the emission line is hot, then the molecules will have a high velocity dispersion, broadening the emission line through minor spectral shifts. These broad emission lines are observed in some AGN, but not all. However narrow emission lines are observed ubiquitously.

This was originally taken as evidence for two distinct populations of active galaxies. However, as with other characteristics, the two were reconciled with a new structure of the AGN geometry. Most important is the lack of spherical symmetry. The

unified model of AGN proposes many of the different AGN observables are due to line of sight geometry rather than intrinsic differences (Orr & Browne, 1982). AGN are often observed with energetic jets located at either pole which can clear gas out of the ISM. This can result in a *torus* of gas and dust around the black hole which can obscure direct observation of the central nucleus (Orr & Browne, 1982). Now, gas responsible for broad emission lines would exist very close to the nucleus being heated by radiation, while narrow emission lines would come from colder gas farther away (Orr & Browne, 1982). Hence BLRs would be obscured from view when the galaxy is oriented properly, while NLRs would be visible regardless (Orr & Browne, 1982). This is the current best model of AGN and the framework in which we assume herein.

While some of the classes of AGN can be explained by geometric orientation of the host galaxy, others seem to comprise physically distinct phases of activity. It is these intrinsically different AGN which are most interesting in regards to galaxy evolution, and may hold important clues to AGN phases and their interplay during the life cycle of the host galaxy.

An example of two physically-distinct phases in AGN activity are Seyferts and LINERS, which exhibit unique emission lines with different excitation properties. In addition to specific spectral signatures, Seyferts and LINERS have been shown to reside in characteristic host galaxies when compared to star forming galaxies and one another (Juneau & Dickinson, 2013). Kauffmann et al. (2003), showed that galaxies hosting AGN typically have larger stellar masses than those that are not.

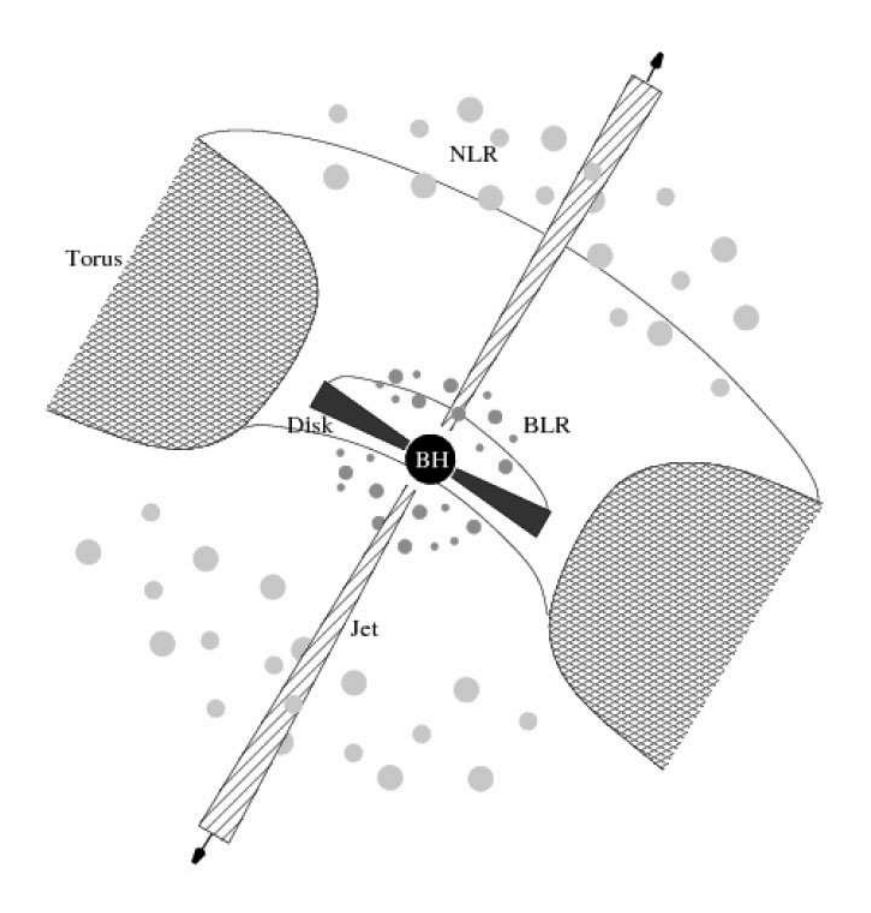


Figure 1–1: AGN Unification model - http://ned.ipac.caltech.edu/level5/March12/Middelberg/Middelberg3.html

Furthermore, galaxies hosting a Seyfert nucleus have a younger stellar population whereas LINERS typically contain older stellar populations as well as larger stellar mass. Therefore it is not a stretch to conclude that Seyferts may comprise the early stages of AGN activity when compared to the more mature LINERS.

This emerging picture of AGN evolution and subsequently galaxy evolution holds true in the local universe but remains to be tested out to higher red-shift. To gain a thorough understanding of the importance of AGN and active phases in the galactic life-cycle, we must extend this picture to the early universe. However, gathering complete samples of active galaxies and distinguishing the powering source is challenging beyond z = 0.4 since traditional emission line diagnostics drift into the IR.

1.3.2 AGN Diagnostics

Typically, the excess luminosity characteristic of AGN is used to identify a galaxy hosting an active nucleus. Specifically, selection by blue optical colour, IR colour, radio or X-ray emission can be used to identify powerful quasars out to very high red-shifts. X-ray emission in particular is a trusted method in diagnosing nuclear activity in powerful AGN, and has been used extensively in recent decades.

As with any other celestial object AGN exist with a spectrum of characteristics defining unique populations, as mentioned above. X-ray diagnostics are less effective on moderately accreting or obscured AGN systems (Juneau et al., 2011). Black holes that are accreting mass at a moderate rate do not exhibit such excessive luminosity and therefore may not produce strong X-ray signals, where emission from AGN surrounded by dense gas and dust may get absorbed. Instead the most efficient method for identifying these AGN relies on the unique emission line signatures produced by all active nuclei. The much higher-ionization radiation from AGN increase the emission line ratios of forbidden lines to hydrogen recombination line, when compared to normal star formation processes (Trump et al., 2013). Furthermore, these lines can be observed in the narrow line regions (NLR) even when the host galaxy's orientation

prevents direct observation of the nucleus. They are therefore a powerful tool for selecting low luminosity and obscured AGN.

In particular, the line ratios $f([OIII]\lambda 5007)/f(H\beta)$, $f([NII]\lambda 6584)/f(H\alpha)$, and $f([SII]\lambda 6718 + 6731)/f(H\alpha)$ are commonly used in the well established "BPT" and "V087" diagrams (Juneau et al., 2011). These forbidden lines are rare in dense gas but can be observed in diffuse gas when excited by ionizing radiation (Trump et al., 2013). Furthermore, due to the aforementioned AGN geometry these lines remain visible even when the X-ray or UV ionizing source is obscured. In addition, due to the close proximity of the lines involved, the ratios are nearly insensitive to reddening allowing them to be used out to high red-shifts. These line ratios also remain visible in low luminosity AGN, which are otherwise dominated by their host galaxy starlight. Therefore optical line ratios are a powerful and robust tool for identifying moderately accreting and obscured AGN.

This method for AGN identification has had wide success in the nearby universe, however extending it to z > 0.4 is difficult because the [NII]/H α and [SII]/H α line ratios shift into the IR wavelength regime (Juneau et al., 2011). Classic AGN diagnostic line ratio diagrams such as the "BPT" and "V087" diagrams require two line ratios to properly distinguish AGN, since a high [OIII]/H β alone is degenerate between nuclear activity and low metallicity.

A solution is to take advantage of the correlation of metallicity with colour and stellar mass, to avoid the second line ratio altogether (Juneau et al., 2011). These new modified diagnostic tools utilize rest-frame colour or stellar mass to replace the observationally troublesome [NII]/H α line ratio, allowing AGN selection beyond z=0.4. Selection using colour-excitation (CEx) or mass-excitation (MEx) diagrams agree well with classic line ratios diagnostics at low red-shift and X-ray selection at high red-shift (Juneau et al., 2011). A complete understanding of galaxy evolution requires studying both stellar populations as well as nuclear activity. Yet differentiating the powering source in a luminous galaxy is not trivial. This is precisely the goal of all star formation (SF)/AGN diagnostic diagrams. Below I will briefly describe the classic BPT and modified MEx diagrams, and show the agreement between the two.

1.4 Mass Excitation Diagnostic

Juneau et al. (2011) introduce the MEx diagnostic tool for identifying moderately-accreting or obscured AGN beyond z=0.4. While replacing the troublesome [NII]/H α line ratio is not a novel idea, using stellar mass to identify nuclear activity has a number of additional benefits. Juneau et al. (2011), use a large sample of nearby galaxies from the SDSS to first calibrate the new tool before comparing it to the well established BPT emission line diagnostic. After calibration, the MEx diagram is then compared using a sample of intermediate red-shift galaxies with emission line and X-ray observations. Below I will summarize the calibration and comparison of the MEx diagram in Juneau et al. (2011), and identify the benefits it

has over traditional diagnostics.

To compare the MEx diagram to the BPT diagram we must first have a basic understanding of the BPT diagram and how it is used. The "Baldwin, Phillips & Terlevich" diagnostic was introduced in 1981 when the classification schemes of AGN were based mostly on selection criteria, morphology and line widths (Baldwin et al., 1981). The BPT diagram was created in an attempt to re-emphasize the classification of AGN on the excitation mechanism (Baldwin et al., 1981). This was done by using the ratios of the strengths of emission lines which indicate excitation with lines that originate from star formation. By using a combination of these line ratios, a parameter space was found that could isolate active galaxies from star burst galaxies thus inferring the radiative source (Baldwin et al., 1981). Multiple line ratios can be used, with common ones being $f([OIII]\lambda5007)/f(H\beta)$, $f([NII]\lambda6584)/f(H\alpha)$, and $f([SII]\lambda6718+6731)/f(H\alpha)$ as mentioned above. However the $f([OIII]\lambda5007)/f(H\beta)$ and $f([NII]\lambda6584)/f(H\alpha)$ ratios are most commonly used in BPT diagrams.

Both $[OIII]\lambda 5007$ and $[NII]\lambda 6584$ probe a combination of the ionization parameter and the gas-phase metal abundance (Trump et al., 2013). Juneau et al. (2011) show, using a large sample of nearby SDSS galaxies, that star forming galaxies form a well defined excitation sequence on the lower left of the classic BPT diagram, while galaxies containing an active nucleus form a plume to the upper right (Juneau et al., 2011). This is caused by a higher ionization parameter and/or higher ionizing radiation only found in galaxies hosting an accreting black hole (Juneau et al., 2011).

The division between starburst galaxies and AGN was developed by Kewley et al. (2001). Galaxies that lie between the two curves seen in Fig. 1-2 (a) are expected to have a mixture of starburst and AGN activity and are therefore termed *composites*.

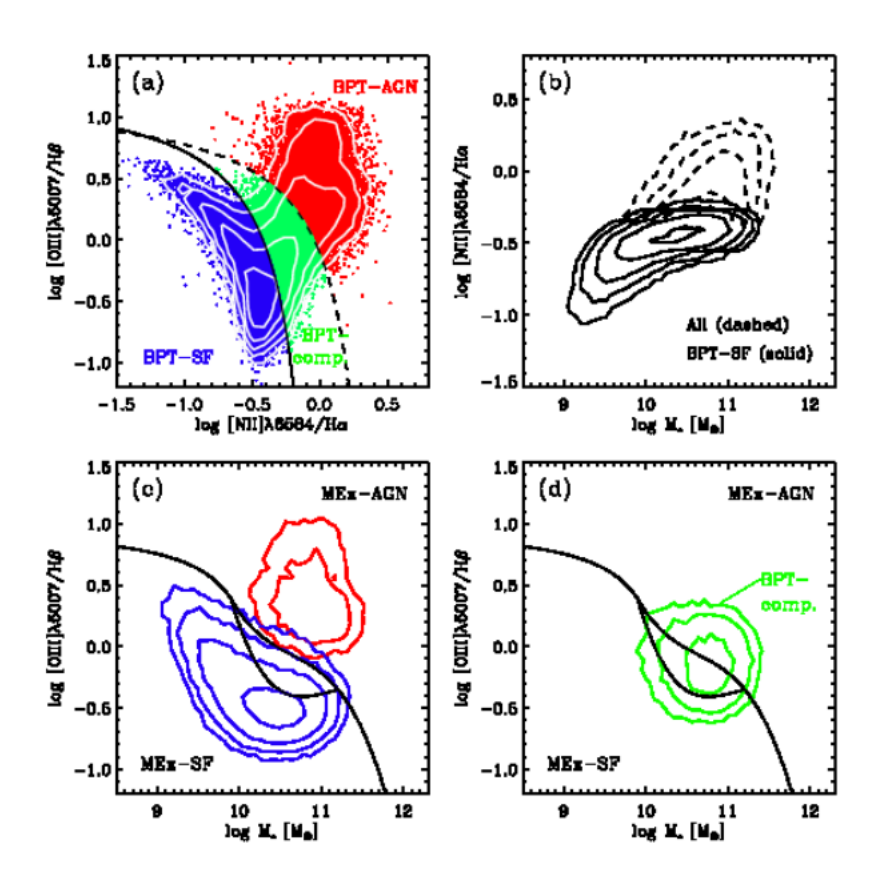


Figure 1–2: Comparison between the classic BPT diagnostic diagram and the newly developed Mass Excitation diagram. In panels c) and d) we can see good agreement between where the BPT (a) populations fall on the MEx parameter space. This is in part explained by the mass-metallicity relation show in panel b). (Juneau et al., 2011)

The first step in developing a suitable alternative to the BPT diagram is finding an accurate parameter in which to replace the redder emission line ratio. The $[NII]/H\alpha$ line ratio is an indicator of the gas phase metallicity in star forming galaxies (Juneau et al., 2011). Now the mass-metallicity relation (seen in Fig 1-2) tells us that there is a physical relation between the aforementioned line ratio and the stellar mass of the host galaxy. Furthermore the $[NII]/H\alpha$ line ratio saturates at high values in normal star forming galaxies, only increasing in the presence of AGN ionizing radiation (Juneau et al., 2011). Similarly AGN have been found to typically reside in galaxies with high stellar masses (Kauffmann et al., 2003). Therefore such systems will exhibit both high $[NII]/H\alpha$ ratios and high stellar mass, placing them in the same quadrant in the BPT diagram and the new MEx diagram. Additionally, stellar mass is a relatively easy parameter to calculate, even for distant galaxies making it an ideal candidate to replace the troublesome $[NII]/H\alpha$ line ratio (Juneau et al., 2011).

Juneau et al. (2011) find strong agreement between the BPT and MEx diagrams. Using the BPT classes as references, the completeness and contamination of the new MEx classes is computed with respect to stellar mass, seen in Fig 1-3. In panel a) we can see that the MEx-AGN classification correctly identifies the BPT-AGN population, reaching close to 100% completeness at high stellar mass. Conversely the contamination of BPT-SF galaxies remains low at all stellar masses, peaking at $\approx 20\%$ for galaxies with $M_{\star} \approx 10^{10} M_{\odot}$, with an average of only 6% contamination. There is, however, significant contamination from BPT-composites, rising steadily with stellar mass. Panel b) then shows us the same comparison but for the galaxies classified as MEx-SF. Completeness is also very high for the star forming class,

near 100%, but has a dramatic drop-off at $M_{\star} > 10^{11} M_{\odot}$. This is most likely due to the fact that at such high stellar mass there are very few purely star forming galaxies (Juneau et al., 2011). Contamination of the MEx-SF class with BPT-AGN galaxies is very low at $\approx 0.3\%$. Again there is significant contamination from BPT-composites, peaking at $\approx 30\%$. We can therefore see that the two classes of AGN and star forming galaxies remain well defined on the new MEx diagnostic, with some contamination from composite galaxies (Juneau et al., 2011). These issues are addressed using probabilistic diagnostics, discussed below.

Juneau et al. (2011) also makes use of the low red-shift sample of SDSS galaxies to calibrate the MEx diagram further. To provide a more useful diagnostic than discrete classification alone, a probabilistic approach is taken. With a *priori* knowledge of the powering source of the SDSS sample, Juneau et al. (2011) calculate the probability a galaxy is classified correctly with respect to its position on the MEx diagram. This is done by first defining four classes: Star-Forming, LINERs, Seyfert 2s, and Composites. The middle two can be distinguished using the [SII]/H α ratio which was available for the calibration sample (Juneau et al., 2011). Then, by defining a sub-sample within a one-sigma box in each parameter (line ratio and stellar mass), the probabilistic classification is defined by the normalized count of each within the box. Juneau et al. (2011) decide to assume LINERs, Seyferts and Composites all have some degree of nuclear activity and therefore define P(AGN) = 1 - P(SF). The distribution of these probabilities can be seen in Fig 1-4. Therefore this classification system has built-in uncertainty which can be utilized for more comprehensive

identification (Juneau et al., 2011).

Finally Juneau et al. (2011) applied the newly calibrated MEx diagnostic to a high-redshift sample of galaxies with multi-wavelength data, specifically X-ray detections. Defining two criteria, an X-ray source was classified as an AGN if it satisfied either 1) $L_{2-10KeV} > 10^{42}erg/s$ or 2) hardness ratio HR > -0.1 (Juneau et al., 2011). Otherwise they were classified as X-ray starbursts. In this way they compared the Mass Excitation diagnostic with a completely independent identification scheme based on X-ray observations. They found that 85% (34/40) of X-ray AGNs with valid emission line measurements (SN > 3) are classified as either MEx-AGN or MEx-composite (Juneau et al., 2011). This shows that the MEx diagram has high success at recovering X-ray identified AGN. Therefore it is possible for surveys lacking X-ray coverage to apply a robust AGN diagnostic using optical spectroscopy out to $z \approx 1$.

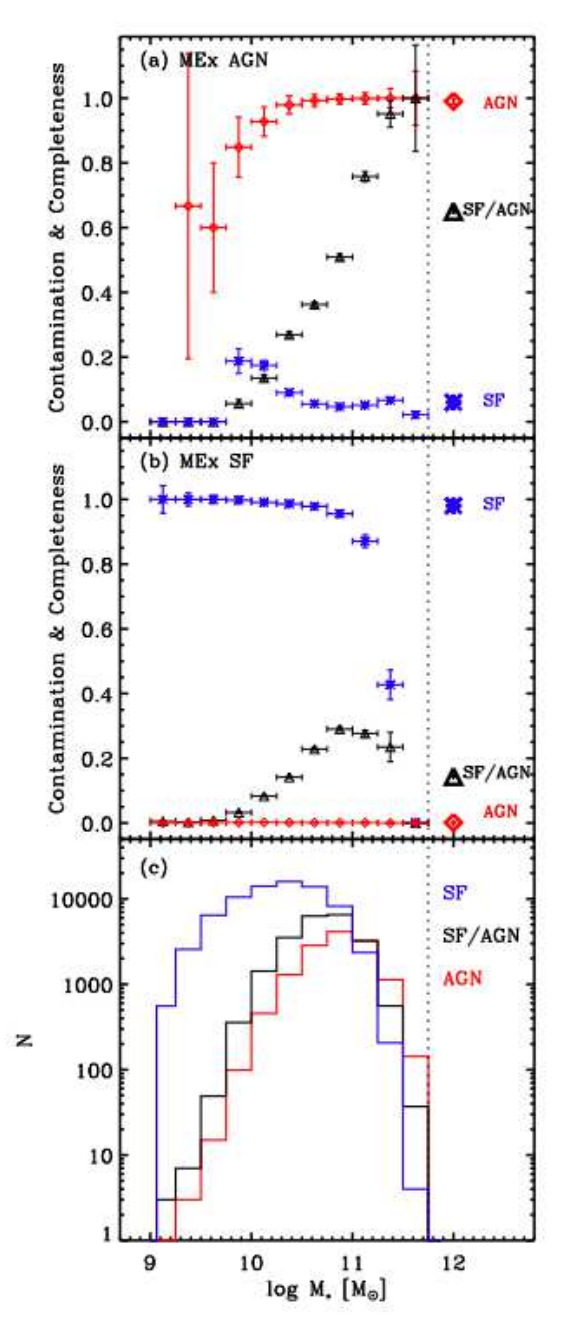


Figure 1–3: Completeness and contamination rates in bins of stellar mass. (Juneau et al., 2011). (a) shows the completeness of galaxies classified as AGN using the MEx diagram and (b) shows the completeness of galaxies classified as star forming.

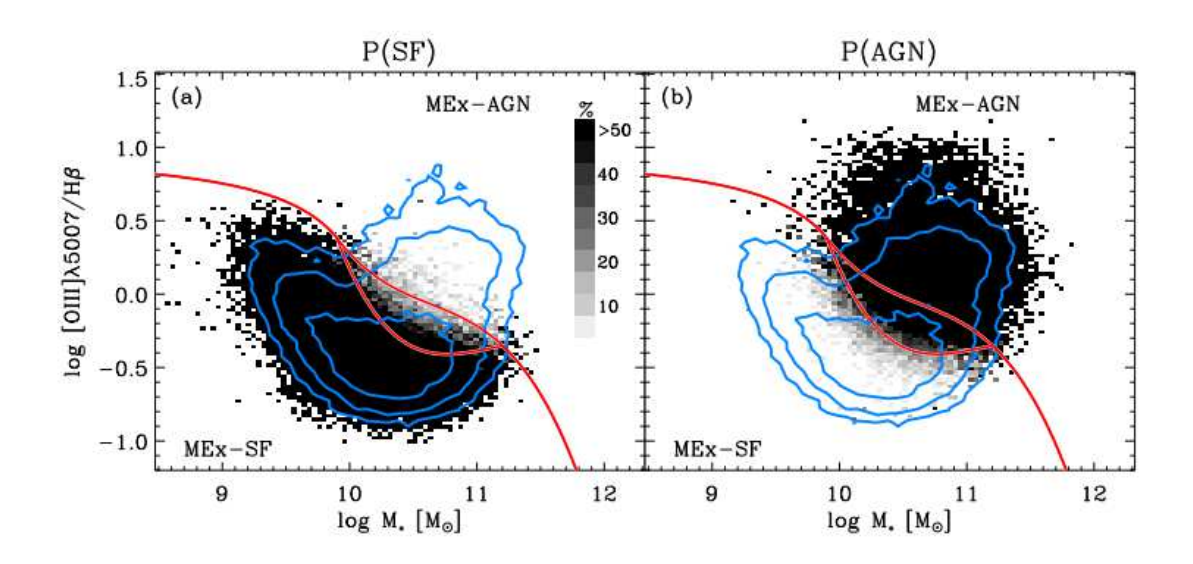


Figure 1–4: Probability of a galaxy being powered by star formation or an active nucleus on the MEx diagnostic. (Juneau et al., 2011). Red lines are the dividing lines separating MEx classified AGN, SF and composite galaxies. Blue contours are areas of equal probability.

CHAPTER 2 Data

The data analysis are based on photometric data of RCS1 taken by Gladders and Yee (2005), and spectroscopic data from IMACS described by Faloon (2013), with some GMOS data. The foundation of the set lies in the Red Sequence Cluster Survey (RCS), described below, with significant follow-up observations having been performed since. Currently the database contains photometric and spectroscopic information that spans the optical and infrared wavelength regimes, with sparse coverage in the x-ray and radio.

2.1 Photometric Observations

2.1.1 Red Sequence Cluster Survey

The Red Sequence Cluster Survey (RCS1) is a $100deg^2$, two filter imaging survey in the R_c and z' filters. The survey was designed to identify and study galaxy clusters up to $z \approx 1.0$, and was observed from 1998-2001 over 13 nights on the Canadian France Hawaii Telescope (CFHT) (Gladders & Yee, 2005). With 22 patches, typically 2.5x2.5 deg, and target depths of 23.8 and 24.9 in the z' and R_c bands respectively, the RCS survey was the largest moderately deep two-filter survey done at the time, and offers a powerful tool in the field of observational cosmology (Faloon et al., 2013). After reduction and processing ≈ 7000 clusters were catalogued in the RCS1 above 3σ . Our study is comprised of a sub-sample of RCS1 clusters for which

spectroscopy and IR imaging was obtained. Below is a comprehensive list of the RCS1 clusters that have coverage in our catalogue.

Cluster	RA	DEC	Redshift
RCS212134	320.391	-63.596	0.217
RCS035139	57.912	-9.940	0.304
RCS144726	221.858	8.471	0.346
RCS132655	201.729	30.351	0.352
RCS022516	36.316	0.191	0.357
RCS092821	142.087	36.775	0.393
RCS022359	35.995	1.435	0.394
RCS145226	223.108	8.576	0.395
RCS051834	79.641	-43.418	0.396
RCS022403	36.012	-2.461	0.408
RCS231526	348.858	-0.778	0.409
RCS044207	70.529	-28.250	0.465
RCS215223	328.095	-5.063	0.480
RCS051855	79.729	-43.250	0.508
RCS110733	166.887	-5.343	0.511
RCS234717	356.820	-36.573	0.538
RCS110104	165.266	-3.855	0.571
RCS144654	221.725	8.455	0.628
RCS144557	221.487	8.671	0.629

RCS110439	166.162	-4.750	0.637
RCS215248	328.200	-6.156	0.649
RCS211852	319.716	-63.576	0.658
RCS110246	165.691	-4.448	0.671
RCS212238	320.658	-61.768	0.690
RCS112225	170.604	24.381	0.709
RCS141910	214.791	53.435	0.710
RCS234220	355.583	-35.571	0.725
RCS044126	70.358	-28.220	0.734
RCS110733	166.845	-5.388	0.735
RCS132939	202.412	28.888	0.758
RCS022433	36.137	-0.038	0.773
RCS110411	166.045	-3.625	0.775
RCS051940	79.916	-44.035	0.827
RCS110118	165.325	-3.476	0.840
RCS110206	165.525	-4.241	0.867
RCS110615	166.562	-3.513	0.868
RCS043936	69.898	-29.078	0.869
RCS162009	245.037	29.490	0.869
RCS022158	35.491	-3.668	0.914
RCS132629	201.620	29.051	0.919
RCS043936	69.898	-29.078	0.956
RCS051908	79.783	-43.388	0.984

Table 1. RCS1 clusters which have complete spectroscopy. Columns describing the cluster name, right ascension, declination and redshift.

2.2 Spectroscopic Data

The Mass Excitation diagnostic requires both spectroscopic and photometric data to properly identify AGN populations. The spectroscopic data within the larger multi-wavelength catalogue has been collected from a number of separate instruments, however after reducing our sample size due to restrictions in redshift space and signal strength (discussed further in Ch. 3), we are left with spectroscopy taken on two instruments. Most of our MEx sources where the necessary emission lines are within the observed wavelength range, as well as those that have strong signal-to-noise ratios, have spectroscopic data that was taken on the Inamori Magellan Areal Camera and Spectrograph (IMACS) on Magellan. The remainder of sources that match our quality criteria were observed on the Gemini Multi-Object Spectrograph (GMOS, north and south).

2.2.1 IMACS

Wide field multi-object spectroscopy was taken with the IMACS instrument on the Baade 6.5 meter Magellan telescope using the University of Toronto's share of Magellan time (Cooper & Yan, 2012). The observations were taken as a part of a large spectroscopic survey covering 43 RCS1 clusters. Each mask was observed in 4x1800s exposures with 650-750 slits per mask, using the IMACS 27' field of view (Faloon et al., 2013). The g150 grism was used with the f/2 camera and 1 arcsecond slit widths, yielding a spectral resolution of R=555 (Faloon et al., 2013). Filter selection was based on the redshift of the target cluster with the aim, with three filters covering z1 = 4250 - 6900Å, z2 = 5150 - 7800Å, and z3 = 6025 - 8675Å (Faloon et al., 2013).

2.2.2 GMOS

Wide field multi-object spectroscopy was taken with the Gemini Multi-Object Spectrograph (GMOS) instrument on the Gemini North 8.1 meter telescope. The R150 grating and RG610 filter combination resulted in spectra from 600-1000 nm, which covers [OII]3727A and importantly [OIII]5007A (along with H β) with a resolution of 250 km/s at $z \approx 0.9$. Therefore, the GMOS spectroscopy provides us the targeted emission lines. However since there is simply much more IMACS spectra in quantity our sample is still dominated by it.

2.3 Sample Selection

When attempting to construct the Mass Excitation diagnostic that will provide us with a tool to identify and then further study galaxies hosting active nuclei, we need both the stellar mass and emission line ratio of the host galaxy. With the stellar mass calculations simply relying on a spectral energy distribution (SED) fit using readily available photometry, it is the emission line spectroscopy which limits our sample. With more complete spectroscopic coverage it would be desirable to originally design a sample that would probe both high and low density environments. However we do not have that luxury and instead are working with a catalogue that was not originally intended for this work. The IMACS spectroscopic survey was designed primarily to get a good sample of optical galaxies for the purpose of finding accurate redshifts for the RCS1 clusters and calculating velocity dispersions and mass measurements to compile a large catalogue of confirmed cluster members. The original plan was to have the IMACS (spectroscopy), MIPS (photometry), and IRAC (photometry) observations cover the same core of RCS1 clusters, but for practical reasons it got split into two separate samples, with ≈ 20 overlapping clusters. The IMACS targets were chosen based on colour to maximize the number of clusters members observed. The filters were chosen for each cluster field to encompass [OII] $\lambda 3727$ to G-band spectral feature, including the ≈ 4000 A Calcium H+K break absorption features. This was based on the estimated photometric redshift of the target cluster.

Since the lines needed for our work lie outside this wavelength window (λ 4861 and λ 5007) we were not able to measure the necessary emission lines for the intended cluster members, and instead turned our attention to alternate sources in the field of view, residing at redshifts which exposed the desired lines. In this way our sample is limited by the chance that the [Olll] and [H β] emission lines were visible to us. Additionally we have to ensure we are only using trustworthy emission lines with acceptable signal-to-noise ratios. These two factors alone reduced the catalogue of \approx 50,000 spectroscopic sources down to 1226 usable MEx candidates, and scientifically

limited the conclusions we can make from an essentially random sample. The details of the signal-to-noise calculation and cut off are described in Ch. 3.

CHAPTER 3 Methods

In order to construct the Mass Excitation diagnostic tool, and classify our sources as either active or star forming galaxies, we must first acquire both the emission line ratios and stellar masses which define the parameter space. As mentioned in Ch 2, the spectroscopy is the limiting variable since the lines are difficult to measure due to weak signal. Therefore we chose to begin by measuring the emission lines of all the spectra available to us, to maintain as strong statistics as possible once our quality cuts were applied.

The scripts developed to measure the emission lines contain the majority of the work in this thesis, and have been designed to be robust and versatile with the hopes of utilizing them for future work.

3.1 Emission Line Measurement

As described in Ch.1, the target emission lines for the MEx diagnostic are $[OIII]\lambda 5007$ and $[H\beta]\lambda 4861$. [OIII] probes a combination of the ionization parameter and the gas-phase metal abundance (Trump et al., 2013). Furthermore, since [OIII] is a forbidden emission line, strong emission at $\lambda 5007$ indicates strong ionizing radiation and is evidence of an active nucleus (Trump et al., 2013). Strong $[H\beta]$ emission on the other hand is an indication of star formation (Trump et al., 2013). Therefore the combined ratio can provide insight into the source of the ionizing radiation. To

arrive at this desired ratio, we must first locate and measure both emission lines.

3.1.1 Equivalent Width

To measure the strength of an emission line, we calculate the *equivalent width*. The equivalent width is defined as the width of a box that has the height of the continuum and the same area as the integrated emission line (Mo et al., 2010). This concept is demonstrated in Fig 3-1.

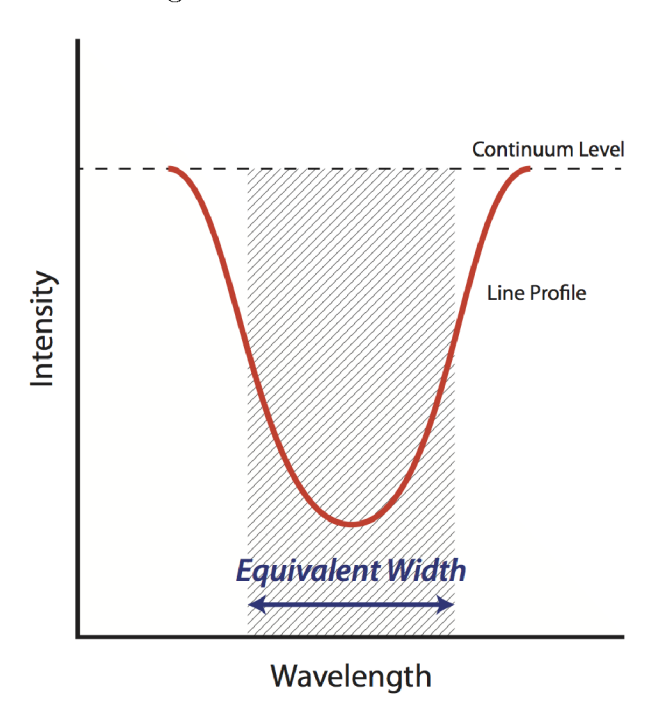


Figure 3–1: The equivalent width of an emission line if the width of a box with the same area as the integrated flux of the emission line, and is used to measure the strength of an emission line (Mo et al., 2010).

The equivalent width is defined in Eq. 3.1 but can be approximated as Eq. 3.2, where W_{λ} is the equivalent width, F_{line} is the integrated emission line flux, and F_{C} is the continuum intensity (Mo et al., 2010).

$$W_{\lambda} = \int \frac{F_{line}(\lambda) - F_{C}(\lambda)}{F_{C}(\lambda)} d\lambda \tag{3.1}$$

$$W_{\lambda} = \frac{F_{line}(\lambda^2)}{F_C(\lambda)} \tag{3.2}$$

Therefore the equivalent width is what we are attempting to measure for both the target emission lines, for each object in the catalogue of spectra.

3.1.2 Line Fitting

To measure the strength of the target emission lines, we therefore need to measure the integrated flux of the emission line. To efficiently deal with the $\approx 50,000$ available spectra, a set of modular IDL scripts were written to handle the different tasks of measuring and checking the entire catalogue of spectra. A thorough quality assurance procedure was applied after the line was fit and measured, described below, but a preliminary quality indication was provided by Ashley Faloon, who originally reduced the raw data. Her quality flag (Q), based on visual inspection, allowed the removal of spectra with excessive noise from the start. Therefore any spectra with $Q \leq 1$ was not considered for measurement.

The measurement process began with first correcting the wavelength to return it to the rest-frame, using the spectroscopic redshift calculated previously by Ashley Faloon. We were then able to check and see if the source was at a redshift that allowed the targeted emission lines to fall within the filter bandwidth. If not the source was discarded as the emission line was unobtainable.

However if the emission line did fall within the filter, we then proceeded to attempt to measure the line. This was done by using an external IDL function, *mfit-peak*, to fit the emission line with a Gaussian curve, taking estimates for the location of the emission line (in angstroms), intensity of the emission line, and variance of the Gaussian function. Subsequently, *mfitpeak* would return a five term estimate of the Gaussian function, along with a linear fit of the continuum surrounding the emission line. Examples of the line fitting can seen in Fig. 3-2.

$$f(x) = Ae^{-(x-\mu)^2/(2\sigma^2)}$$
(3.3)

$$g(x) = mx + b (3.4)$$

Above in Eq 3.3 we can see the standard definition of a Gaussian function, where σ is the variance, μ is the mean, and A is the amplitude. Similarly in Eq. 3.4 we have the simple linear equation to fit the continuum where m is the slope and b is the y-intercept.

mfitpeak Resu	ult Gaussian/Linear Term	Explanation
A[0]	A	Peak Amplitude
A[1]	μ	Peak Centroid
A[2]	σ	Gaussian Sigma
A[3]	b	Linear y-intercept
A[4]	m	Linear Slope

Therefore *mfitpeak* fit both the surrounding continuum and emission line with a linear and Gaussian function respectively, providing us with a five term result. Referring back to Eq. 3.2, we only need the integrated line flux and continuum intensity to arrive at the desired *equivalent width*. Evaluating the linear continuum fit at the location of the emission line provides us with the continuum flux, and the known integral of a Gaussian (Eq 3.5) makes calculating the line flux trivial. In this way, we were able to calculate the *equivalent width* of the desired emission lines for every available spectra.

$$\int Ae^{-(x-\mu)^2/(2\sigma^2)}dx = A\sigma\sqrt{2\pi}$$
(3.5)

3.1.3 Signal-to-Noise

While calculating the equivalent width of the emission line we also had to measure the strength of the emission line in comparison to the surrounding noise of the spectra. Once done measuring the emission lines we need a measure of how trustworthy the line is, and this is called the *signal-to-noise ratio*. It is a rather simple calculation but is imperative to the quality control of our sample, when later deciding on what sources to include on our MEx diagram. A good example of the importance

of this measure can be seen in Fig 3-2, where we compare a clean spectra with strong lines, to a very noise spectra where the lines are barely visible. Seen at the top right of each image is the S/N ratio. We can see the strong lines have S/N > 9, while the weak emission lines surrounded by a lot of noise have S/N < 1.

To calculate the S/N ratio, we first remove the emission line leaving us with the noise from the continuum on either side. As a measure of the strength of the noise, we then take the *standard deviation* of the remaining spectra. Shown in Eq. 3.6, the amplitude of the Gaussian fit described above, taken to be the strength of the *signal*, is divided by the standard deviation of the noise. This gives us a robust measure of the strength of the signal compared to the relative noise, and provides us with a parameter for quality control.

As discussed previously, our initial quality cut came from the quality flags placed on the spectra when they were originally being reduced by Ashley Faloon. Disregarding sources that were at improper redshifts for the target emission lines to fall within the filter window, we were left with our entire catalogue of spectroscopic sources, with measured $H\beta$ [4861] and O[lll][5007] emission lines. Finally, we applied a quality cut of S/N > 4 to ensure strong lines with minimal noise. We arrived at this value by visual inspection, examining at what level signal/noise we could trust the fit of the emission line. This significantly reduced the sample size, since both emission lines

of a spectra had to meet the quality cut. Therefore through this process our sample went from $\approx 50,000$ spectroscopic sources to 1226 usable Mass Excitation sources.

3.2 Stellar Masses

The stellar masses were estimated in the following way. We used the observed IRAC channels 1 and 2 as an approximate measure of the rest-frame K-band luminosity; for galaxies with z < 0.78 we employed the 3.6 micron data and for galaxies with z > 0.78 we used the 4.5 micron data, to most closely approach 2.12 microns in the rest-frame. We did not attempt a K-correction since for most of the galaxies this would be a small (order unity) and uncertain adjustment. We then adopted the colour-specific mass-to-light ratios of Bell & McIntosh (2003); Bell & de Jong (2001) to convert the rest-frame K-band luminosities to stellar masses. This procedure assumes a 'diet' Salpeter Initial Mass Function, which gives a 30% lower mass estimate than the standard Salpeter IMF. Given the observational uncertainties, limited photometric information, and variations in the IMF, we estimate the uncertainty in these estimates is roughly 50%.

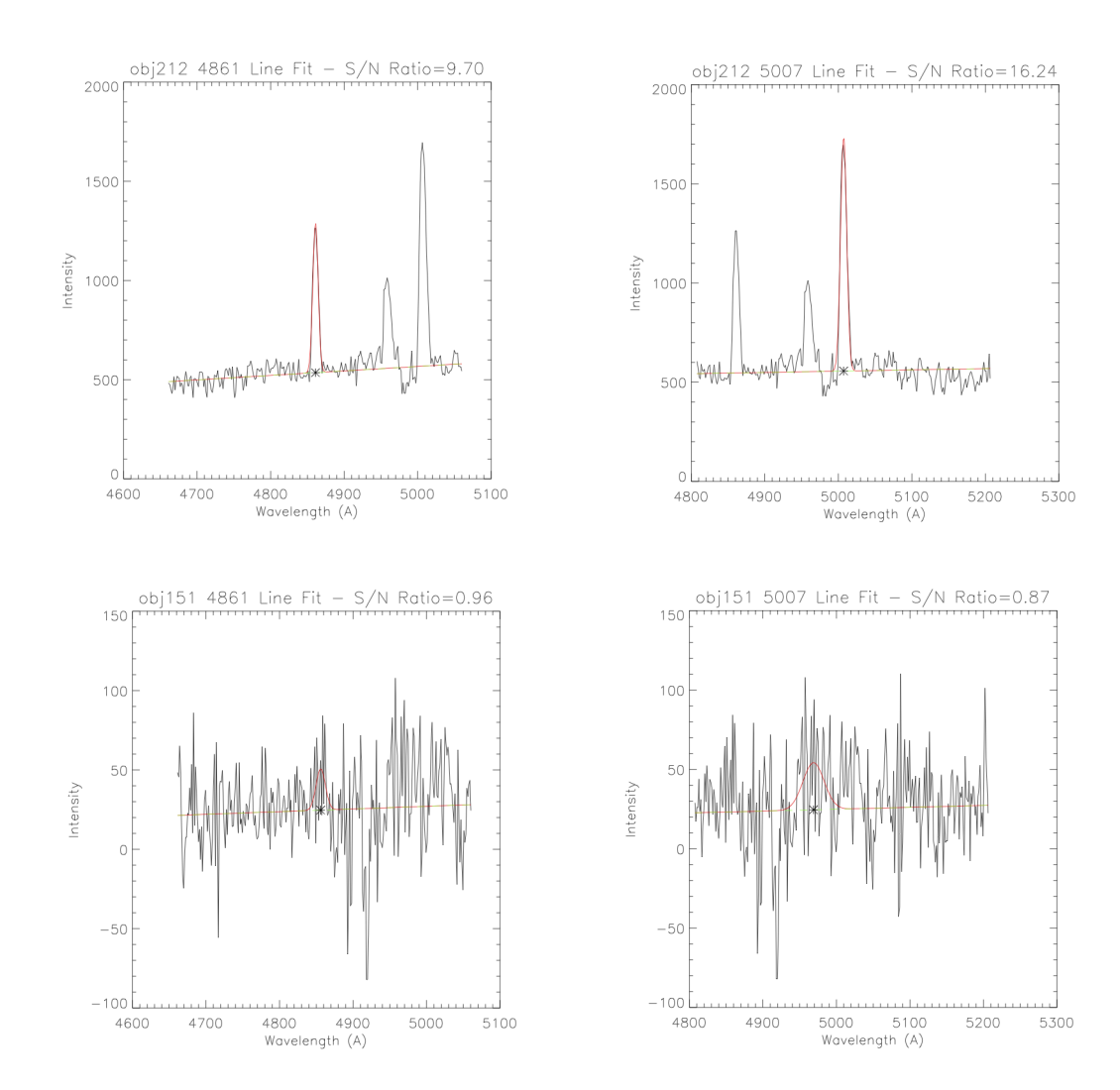


Figure 3–2: Emission line fit for two examples of spectra. The first two are from a high quality spectra, where you can clearly see the guassian function fit over the emission line as well as the continuum fit. The second two are from a spectra with significant noise, which did not pass the quality cut.

CHAPTER 4 Results

4.1 Mass Excitation Diagnostic and AGN Identification

With the measured equivalent widths and subsequent emission line ratios of $f([OIII]\lambda 5007)/f(H\beta)$, and stellar masses of the 1226 quality MEx candidates in hand, we are now prepared to construct and use the Mass Excitation diagnostic to identify active nuclei within our sub-sample. The MEx diagnostic can be seen in Fig. 4-1 with the red symbols identifying the AGN population in the upper right, the blue symbols for the star forming galaxies in the bottom left, and the green symbols for the composite galaxies in the middle. The dividing line is taken from Juneau et al. (2011) and is shown in Eq. 4.1, with the lower curve defined in Eq. 4.2.

$$y(\mathbf{x})=0.37/(\mathbf{x}-10.5)+1 \quad \text{if } \mathbf{x} \leq 9.9$$

$$y(\mathbf{x})=a_0+a_1x+a_2x^2+a_3x^3 \quad \text{otherwise}$$

$$[a_0,a_1,a_2,a_3]=[594.753,167.074,\ 15.6748,0.491215]$$

$$(4.1)$$

$$y(x) = 800.492217.328x + 19.6431x^2 \ 0.591349x^3 \quad 9.9 < x < 11.2$$
 (4.2)

With our three populations defined, the first thing to do is look at the basic numbers from these classifications, shown in the table below. We see that the majority of sources have been classified as star forming galaxies with 67% of the MEx sources, with about half that, 30% being active galaxies. The remaining 3% are composite galaxies that are assumed to have both star formation and an active nucleus.

Population	Description	Number	Percent
AGN	hosting active nuclei	371	30%
Star Forming	ongoing star formation	820	67%
Composites	evidence of both	35	3%

Table 2. Results of MEx diagnosis, showing a majority star forming galaxies.

The significant fraction of our sample diagnosed as star forming is on one hand expected since star forming galaxies are more common than AGN (Georgakakis & Nandra, 2008), but also suspect due to the questionably low stellar masses of our sample. The stellar masses were calculated using a rudimentary approach, fitting spectral energy distributions (SEDs) using the photometric data we have, leading to very high uncertainties. Upon inspection we have a large number of sources with unexpectedly low stellar masses (Juneau et al., 2011). We cut the MEx diagram at $M_{\star} < 8$ deciding that anything below was untrustworthy. This suggests that further

time needs to be spent on the stellar masses with a more sophisticated approach, as is discussed in the following chapter.

4.2 Redshift Distribution

Our next step in taking a closer look at the characteristics of the different populations classified using the MEx diagnostic is examining the redshfit distributions. These distributions can be seen in Fig. 4-2. When looking at the redshift distributions, we are looking for any differences to indicate an evolutionary significance over cosmic time.

Eastman et al. (2007) found that the X-ray fraction of galaxies hosting an active nucleus rapidly increases between $z \approx 0.2$ and $z \approx 0.6$. Galametz et al. (2009) further quantified the AGN fraction increase based on surface density measurements of X-ray, MIR, and radio AGN. Martini et al. (2009) demonstrated that the AGN fraction increases as $(1+z)^{5.3}$ for AGN above a hard X-ray luminosity of $L_X \geq 10^{43} erg/s$. Furthermore the rapid rate of AGN evolution was shown by Haines et al. (2009) to resemble the evolution of the fraction of star forming galaxies in clusters $f_{SF} \propto (1+z)^{5.7}$. Evidence points towards a correlation between the evolution of star formation and nuclear activity, yet the extent and details of this relationship are still unclear (Martini et al., 2009).

When looking at the redshift distributions it might be tempting to say we also see an increase in AGN fraction from 0 > z > 4, yet this is a global count and not the AGN fraction. When normalized by the entire sample, see Fig. 4-3, we can see that

the AGN and star forming population fractions remain relatively constant. Visually this is apparent as all three populations follow roughly the same distribution. This is most likely due to the sample selection method, and will be discussed in detail in the following chapter.

4.3 Colour Evolution

Finally we can examine the MEx identified populations using a *colour-magnitude* diagram (CMD), a well established method for analysing populations of galaxies. In the CMD we use two bands of photometric imaging taken on the CFHT Megacam to calculate the colour of a galaxy. CMDs can be made with different photometric bands but here we use the z' band (890 nm) and the R band (625 nm) (Gladders & Yee, 2005).

This distinction is important because commonly two characteristic populations are observed on the CMD, the red sequence and the blue cloud. Referring back to Ch.1 where the general characteristics of the generic blue vs red galaxies are described, we remember that typically blue galaxies are younger galaxies still exhibiting star formation, while "red and dead" galaxies tend to be large, evolved ellipticals with little star formation.

Therefore, in terms of the evolution of a galaxy, the CMD is an important and relatively easy tool to evaluate the current evolutionary phase. Moreover, recently a number of studies have attempted to gain insight into the AGN and its role in transforming galaxies using colour as a probe. As active galaxies have gained more attention recently, so has the relationship between the active nuclei and star formation.

Georgakakis & Nandra (2008) explore the role of AGN in "establishing and maintaining the bimodal colour distribution". Theoretically the feedback from active black holes can quench star formation by heating up and/or dispersing the cold gas needed as fuel, hence causing their transition from the blue cloud to the red sequence (Georgakakis & Nandra, 2008). Georgakakis & Nandra (2008) test this idea by examining the X-ray properties of galaxies in the transitional "green valley", and the incidence of AGN in post-starburst galaxies. In doing so they find that i) there is evidence for AGN activity in galaxies found in transition, ii) there is a relationship between nuclear activity and post-starbursts at $z \approx 0.8$, and iii) AGN activity outlasts star formation, with many active galaxies residing in the red sequence (Georgakakis & Nandra, 2008).

Further studies have provided additional evidence for this picture of the transformative role of AGN in a galaxy's life cycle (Shabala et al., 413). Pović (2012) conclude that X-ray selected AGN in the "green valley" present a transition population, quenching star formation through numerous feedback mechanisms and evolving into red sequence ellipticals. They also look at the host morphology and add that there is evidence for major and minor mergers triggering such active phases (Pović,

2012). This is of particular interest when framed in the context of high density environments where triggering interactions would be much more likely. Therefore there is evidence for AGN playing an important role in triggering evolutionary change in young galaxies by quenching star formation.

However when examining the CMD produced with our sample in Fig. 4-4, we observe some unexpected results, that do not immediately agree with this simple story. First, we do not see any discernible difference between the AGN and star forming populations in terms of where they exist on the CMD. However more importantly we see both occupying, almost exclusively, the blue cloud. This is very interesting and unexpected, as traditionally we expect to see star forming galaxies in the blue cloud and AGN in the red sequence, or perhaps the blue cloud (Mo et al., 2010). This peculiar result may be a product of selection effects (discussed below), or may indicate that the evolutionary picture is more complicated.

Rovilos & Georgantopoulos (2007) study the optical colours of X-ray sources from the Extended Chandra Deep Field South (ECDFS), and find that X-ray sources populate both the blue cloud and the red sequence on the colour magnitude diagram. Similarly, Schawinski & Urry (2014) use a low redshift sample to study the quenching of star formation, however not specifically in regards to AGN. They argue that the "green valley" in between the red and blue populations is not a single transitional state. Their analysis, which takes into account morphology, shows that only a small number of blue early-type galaxies move quickly across the green valley after star

formation is rapidly quenched (Schawinski & Urry, 2014).

Turning our attention back to our sample, this latter evidence appears to provide stronger agreement. One important difference that is evident is that the majority of previous work has been done using X-ray sources, which can represent an intrinsically different population of AGN. However we can see that there is evidence both for and against the idea of AGN as a rapid transformational agent. This suggests that the role AGN play in initiating and sustaining galaxy evolution is more complicated than a simple shut-off switch for star formation.

We observe both populations identified from the MEx diagram occupying the blue cloud. We must consider the possibility that the diagnostic misidentified our sources and in reality our entire sample consists of blue star forming galaxies, providing the ionization for the emission lines measured. With that stated however, we can speculate as to mechanism which may result in the majority of our AGN sample residing in blue galaxies. A galaxy exhibiting a blue colour is usually indicative of a young stellar population. This is because young stars emit strongly in the UV and blue end of the optical regime (Mo et al., 2010). Therefore, if we trust the diagnostic, we appear to have a sample of AGN residing in host galaxies with relatively young stars.

Kauffmann et al. (2003) study the properties of the host galaxies of $\approx 22,600$ narrow-line AGN in the nearby universe from the SDSS. Focusing on the luminosity

of the O[lll] emission line as a tracer for the strength of nuclear activity, they find that a young stellar population is general property of AGN with high O[lll] luminosities (Kauffmann et al., 2003). When you consider that the spectroscopic catalogue in which our sample originated was not taken for the purpose of this study, the young age of our classified AGN begins to make sense.

The spectroscopy was taken as a part of a much larger survey whose priority was to retrieve as many redshifts as possible. This meant that the integration time was chosen to be a small as possible, leading to the significant noise seen in the spectra. Therefore when attempting to measure both emission lines through the surrounding noise, it is reasonable to assume only the most luminous O[lll] lines made the quality cut. Our sample of blue AGN could then be a result of the selection bias implemented by the quality of our spectra, yet can still lend evidence in support of Kauffmann et al. (2003).

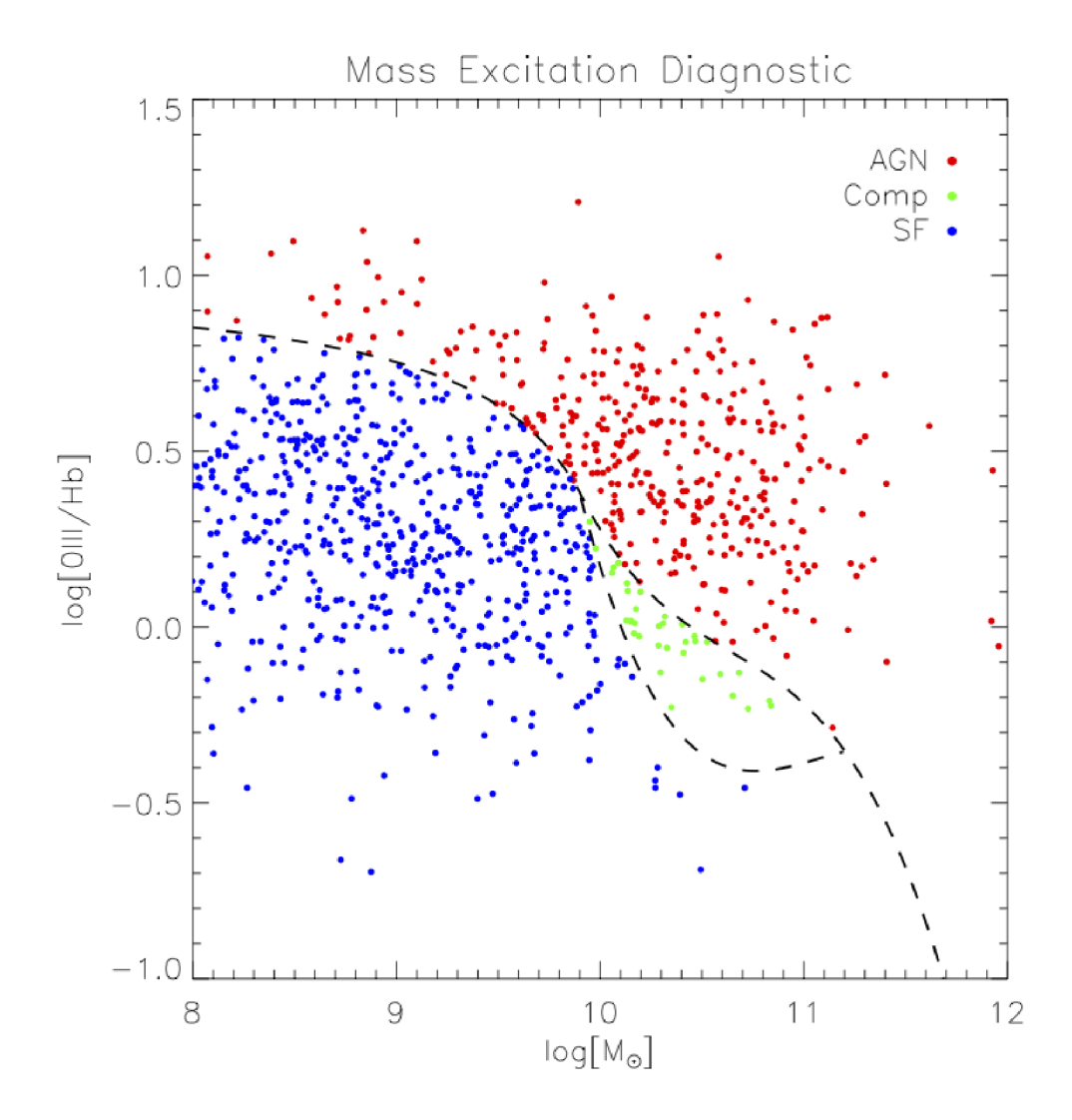


Figure 4–1: The Mass Excitation Diagnostic tool. With the $f([OIII]\lambda 5007)/f(H\beta)$ line ratio on the y-axis and M_{\star} on the x-axis, Juneau et al. (2011) define three distinct regions identifying galaxies with active nuclei (top right), star forming (bottom left) and composites (middle). Our sample exhibits suspiciously low stellar masses, discussed below.

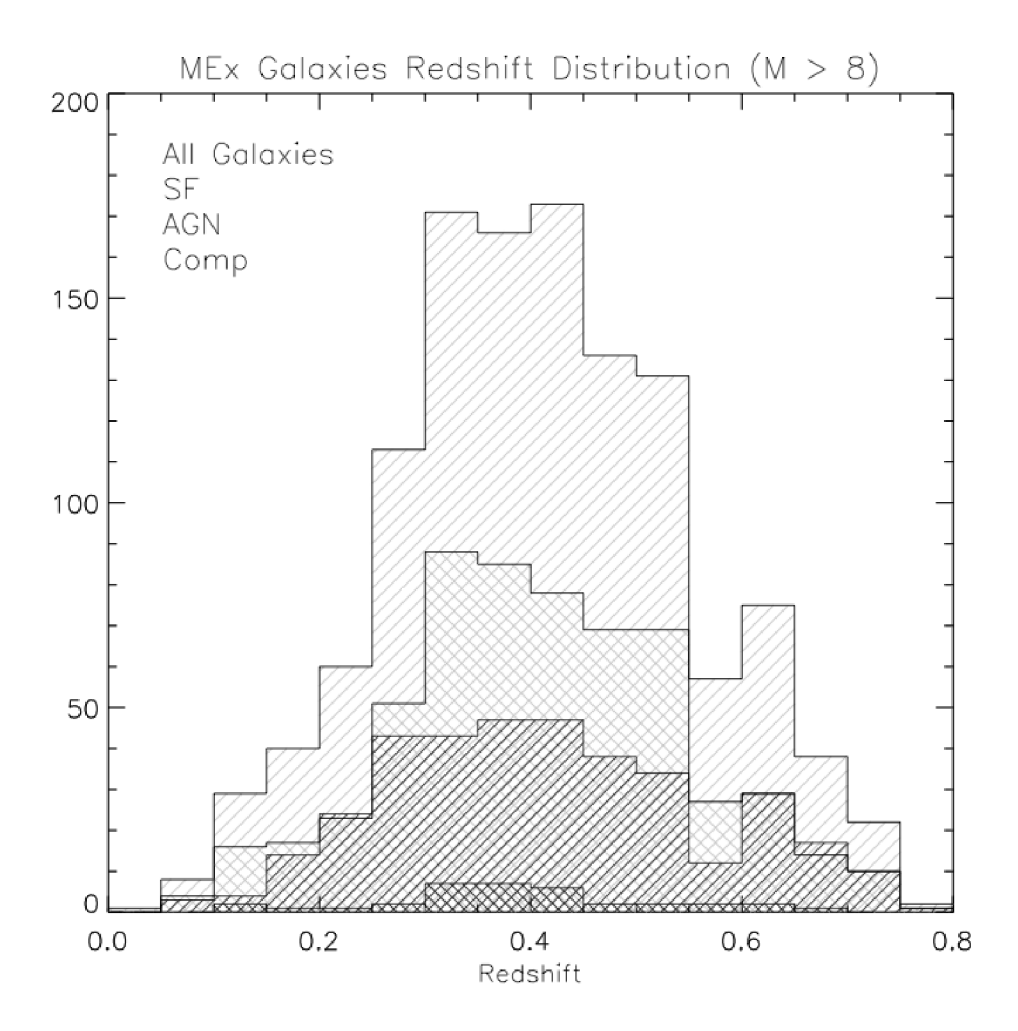


Figure 4–2: Redshift distribution of the three different populations identified by the MEx diagnostic. In descending order the distributions are are: all galaxies, star forming, AGN, and barely seen are the composites. A difference in redshift is not seen here.

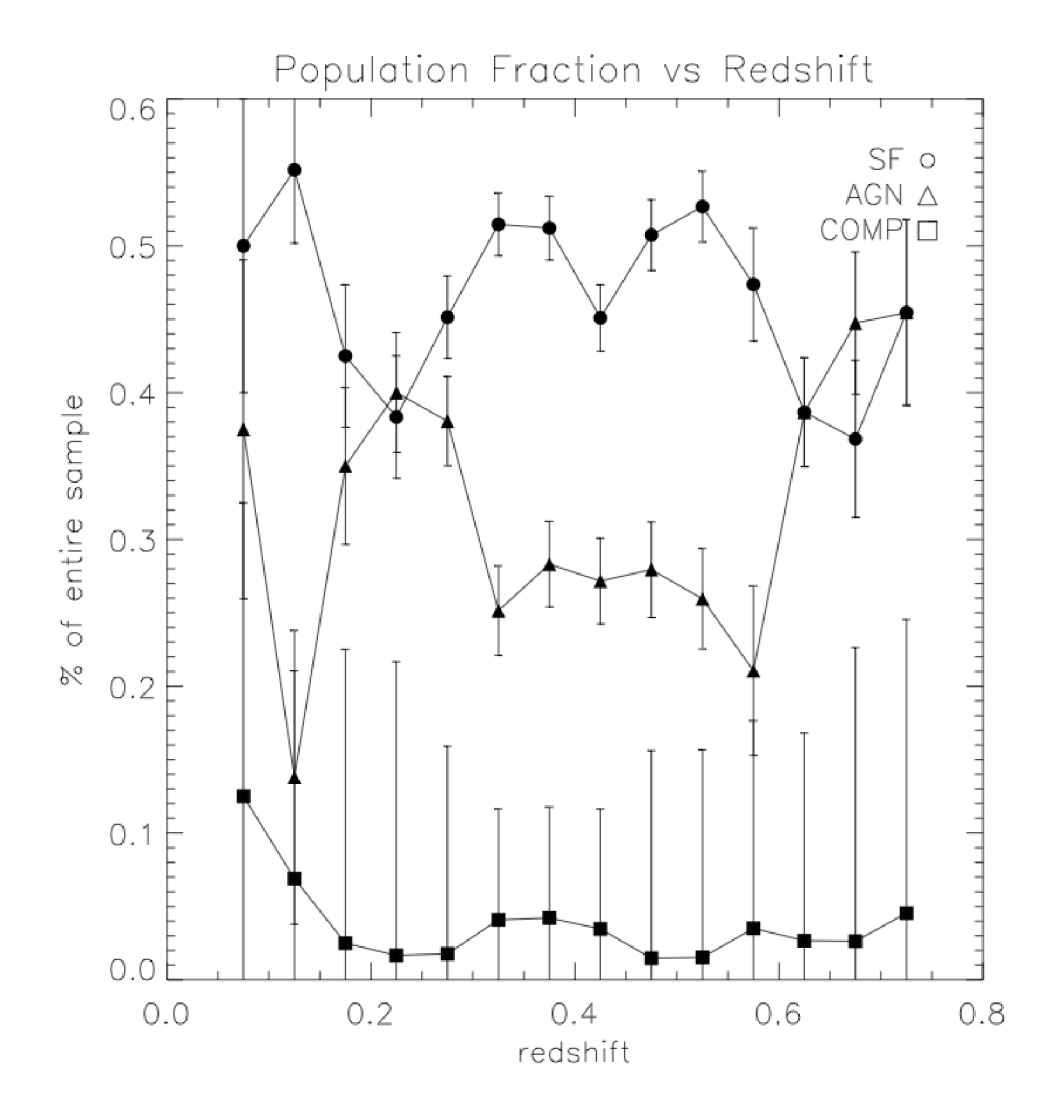


Figure 4–3: Comparison of the three different populations, as a percent of the entire sample population in redshift bins of z=0.05. This further emphasizes that there is no significant trends over redshift space as each population remains relatively unchanged.

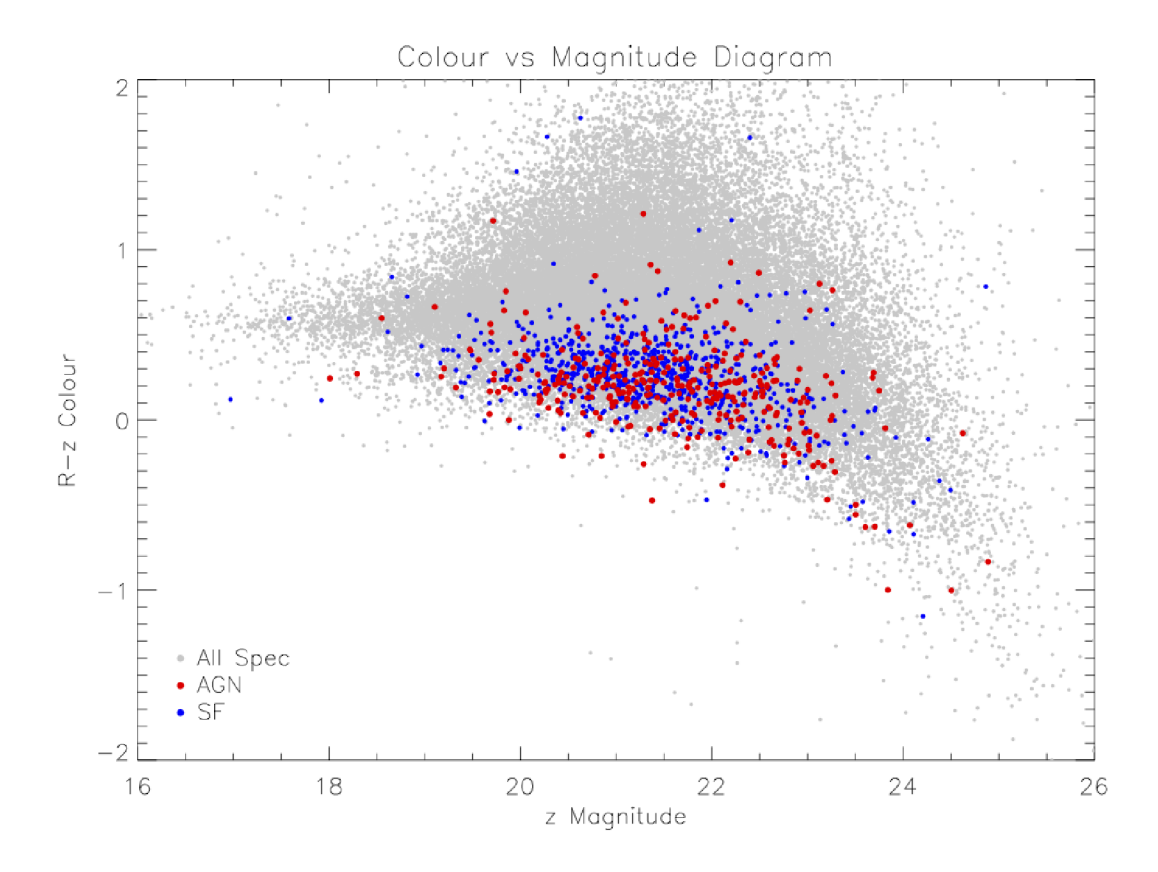


Figure 4–4: Colour vs Magnitude diagram. R-z' colour is on the y-axis with z' magnitude on the x-axis. MEx AGN are in red, MEx SF are in blue, and all spectroscopic sources ($\approx 50{,}000$) are shown in grey. We can see that both the AGN and SF galaxies both occupy the "blue cloud". Furthermore we do not see any evident significant differences between the two populations.

CHAPTER 5 Conclusion

Unfortunately upon reflection this study leaves something to be desired. Beginning with ambitious goals a number of roadblocks, most prominently with the source data, hindered the reach of the available analysis. However with the methods in place, and the scripts developed, future work remains promising.

5.0.1 Quantitative Conclusions

- From $\approx 50,000$ spectroscopic sources, we were successful in measuring the equivalent widths of the O[lll] and H β emission lines for 1226 sources with $\sigma > 4$
- The Mass Extinction Diagram introduced by Juneau & Dickinson (2013) can be used to identify AGN in the absence of the [NII]/H α line ratio, therefore allowing for identification at redshifts greater than 0.4.
- We confirm the relationship seen by Kauffmann et al. (2003) that strong [OIII] line emission is indicative of active nuclei residing in galaxies with young stellar populations.
- We have therefore identified a population of young active galaxies at high redshift, that can be used for further studies in environmental galaxy evolution analysis.

5.1 Future Work

5.1.1 Sample Selection and Design

The source of the majority of the problems faced during this study was the fact that the data itself was not originally observed with this work in mind. Of course everyone does not have the luxury of access to telescope time, particularly during a masters. However with the proper planning and sample design, the methods employed here could provide powerful insight into galaxy evolution and the role of active galaxies.

As mentioned previously, it is hard to take many meaningful results from our sample of essentially randomly selected galaxies. The spectroscopy available to us was taken with minimal integration times, since it was intended mainly for finding redshifts, which does not require high quality spectra. Therefore when searching for quality emission lines (two of them) our sample was dictated by whichever lines were strongest, being able to be properly measured above the noise. This led to a sample based on strength, not scientifically designed with our goal in mind.

With the opportunity to design a sample from scratch, we would be able to properly probe different cosmic environments and achieve appropriate levels of noise, allowing us to place all galaxies on the mass excitation diagnostic, hence accurately representing the intrinsic populations. Reducing selection effects as much as possible would allow for much more robust conclusions, and minimal speculation.

Specifically it would be ideal to probe a broad range of environments, perhaps observing galaxies in the field, groups and clusters. Furthermore, another worthwhile effort would be to examine the evolution of the AGN and star forming populations across redshift space, determining the fractions residing in high density clusters. Initially we hoped to be able to include such analysis in this study, but it is imperative to trust your sample and the methods used to arrive at ours did not allow us to.

5.1.2 Environmental Analysis

Originally the focus of the study was environment and how the high density habitat of a cluster affected the evolution of galaxies. Unfortunately we were not able to delve into this topic due to time constraints and lack of information. This however remains an intriguing and promising research opportunity.

5.1.3 Stellar Masses

Finally, the stellar masses, calculated by photometric SED fits, were questionably low and gave us reason to doubt the MEx results. Although we chose not to include them on the MEx diagnostic, a large amount of sources had $M_{\star} < 10^8 M_{\odot}$ which is uncharacteristically low. A quick rudimentary method was used to calculate the masses, and therefore we must also question the accuracy of the remaining stellar masses. If revisited, a more thorough and robust calculation would be desired.

5.1.4 Conclusion

Galaxy formation and evolution continues to be one of the most exciting and promising areas of study in cosmology today. Large steps have been taken in recent decades towards understanding the fundamental governing mechanisms which result in the wide variety of galaxies we observe in the night sky. However much work remains to be done, and in this study we have highlighted some of the most promising techniques for doing so. As technology continues to improve, large scale surveys like the RCS become more economical, as do space-based observations, and our ability to peer ever further into the cosmic time line grows accordingly.

Due to the diverse populations of galaxies observed, when studying galaxy evolution one of the strongest tools available is statistically large samples. These allow us to compare and contrast the characteristics of entire populations, in turn gaining a better understanding of the relationships between them. Through the course of this study that was the intent, to use the existing catalogue built over multiple observations and surveys, to identify and characterize galaxies hosting active black holes and use them as a indicator of the evolutionary phase of those galaxies.

From our sample of $\approx 50,000$ spectroscopic sources, we were successful in measuring the equivalent widths of the O[lll] and H β emission lines for 1226 sources with $\sigma > 4$, and subsequently calculating the indicative line ratio between the two. Utilizing Juneau et al. (2011)'s novel Mass Excitation Diagnostic tool, replacing the [NII]/H α line ratio with the comparable stellar mass, we identified 371 active galactic

nuclei, comprising 30% of our subsample.

Unfortunately we were not able to identify any observable differences between the active population and the remaining star forming galaxies, in both redshift distribution and colour-magnitude space. However we did find that all galaxies, regardless of the ionizing source occupied the blue cloud on the colour-magnitude diagram. This is surprising, as we would expect to see a significant amount of the AGN residing in the red sequence. This can be explained as a selection effect, since our quality criteria preferentially selected sources with particularly strong O[lll] emission lines, which are known to have young stellar populations (Kauffmann et al., 2003). We therefore have identified a population of young galaxies that have luminous active nuclei residing at their center.

The potential for future work, utilizing the processes and scripts developed here, is promising and exciting. With a more intentional and complete data set, the MEx diagram will be a powerful tool for gaining a better understanding of galaxy evolution and the role of the active nucleus.

References

- Abel, T., Anninos, P., Zhang, Y., & Norman, M. 1997, Modeling primordial gas in numerical cosmology, New Astronomy, 2, 181
- Antonucci, R. 1993, Unified Models for Active Galactic Nuclei and Quasars, Annual Review of Astronomy and Physics, Vol. 31, 473
- Arag, A., Baugh, C. M., & Kauffmann, G. 1998, The K-band Hubble diagram for the brightest cluster galaxies: a test of hierarchical galaxy formation models, Monthly Notices of the Royal Astronomical Society, 434, 427
- Arnold, T. J., Martini, P., Mulchaey, J. S., Berti, A., & Jeltema, T. E. 2009, Active Galactic Nuclei in Groups and Clusters of Galaxies: Detection and Host Morphology, The Astrophysical Journal, 707, 1691
- Atlee, D., Martini, P., & Assef, R. 2011, A Multi-Wavelength Study of Low Redshift Clusters of Galaxies I. Comparison of X-ray and Mid-Infrared Selected AGNs, The Astrophysical Journal, 729
- Baldwin, J., Phillips, M., & Terlevich, R. 1981, Classification Parameters for the Emission-line Spectra of Extragalactic Objects, Publications of the Astronomical Society of the Pacific, 93, 5
- Barger, A. & Cowie, L. 2001, Supermassive black hole accretion history inferred from a large sample of Chandra hard X-ray sources, The Astronomical Journal, 122, 2177

- Bell, E. & McIntosh, D. 2003, A first estimate of the baryonic mass function of galaxies, The Astrophysical Journal, 1
- Bell, E. F. & de Jong, R. S. 2001, Stellar Mass-to-Light Ratios and the Tully-Fisher Relation, , 550, 212
- Conselice, C., Gallagher, J., & Wyse, R. 2002, Galaxy Populations and Evolution in Clusters. II. Defining Cluster Populations, The Astronomical Journal, 123, 2246
- Cooper, M. & Yan, R. 2012, The Arizona CDFS Environment Survey (ACES): A Magellan/IMACS Spectroscopic Survey of the Chandra Deep Field-South, Monthly Notices of the Royal Astronomical Society, 425, 2116
- Eastman, J., Martini, P., Sivakoff, G., Kelson, D. D., Mulchaey, J. S., & Tran, K.-V. 2007, First Measurement of a Rapid Increase in the AGN Fraction in High-Redshift Clusters of Galaxies, The Astrophysical Journal, 664
- Efstathiou, G. & Silk, J. 1983, The formation of galaxies, , 9, 1
- Faloon, A., Webb, T., & Ellingson, E. 2013, The Structure of the Merging RCS 231953+00 Supercluster at z~0.9, The Astrophysical Journal, 768, 104
- Fixsen, D. J. 2009, The Temperature of the Cosmic Microwave Background, The Astrophysical Journal, 707, 916
- Galametz, A., Stern, D., Eisenhardt, P. R. M., Brodwin, M., Brown, M. J. I., Dey, A., Gonzalez, A. H., Jannuzi, B. T., Moustakas, L. a., & Stanford, S. A. 2009, The Cosmic Evolution of Active Galactic Nuclei in Galaxy Clusters, The Astrophysical Journal, 694, 1309
- Gamow, G. & Teller, E. 1939, On the Origin of Great Nebulae, Physical Review, 55, 654

- Georgakakis, A. & Nandra, K. 2008, The Role of AGN in the Colour Transformation of Galaxies at Redshifts z1, Monthly Notices of the Royal Astronomical Society, 385, 2049
- Gladders, M. D. & Yee, H. K. C. 2005, The RedSequence Cluster Survey. I. The Survey and Cluster Catalogs for Patches RCS 0926+37 and RCS 1327+29, The Astrophysical Journal Supplement Series, 157, 1
- Haines, C., Smith, G., & Egami, E. 2009, LOCUSS: The Mid-Infrared Butcher-Oemler Effect, The Astrophysical Journal, 704, 126
- Harrison, E. R. 1970, Fluctuations at the Threshold of Classical Cosmology, 1, 2726
- Hawking, S. W. 1982, The development of irregularities in a single bubble inflationary universe, Physics Letters B, 115, 295
- Hickox, R. 2009, The Big Picture of AGN Feedback: Black Hole Accretion and Galaxy Evolution in Multiwavelength Surveys, AIP Conference Proceedings, 1201, 13
- Hickox, R. C., Jones, C., Forman, W. R., Murray, S. S., & Kochanek, C. S. 2009, Host Galaxies, Clustering, Eddington Ratios, and Evolution of Radio, X-Ray, and Infrared-Selected AGN, The Astronomical Journal, 696, 891
- Hopkins, P. & Hernquist, L. 2005, Black Holes in Galaxy Mergers: Evolution of Quasars, The Astrophysical Journal, 630, 705
- Jones, B. & Wyse, R. 1985, The ionisation of the primeval plasma at the time of recombination, Astronomy and Astrophysics, 149, 144
- Juneau, S. & Dickinson, M. 2013, Widespread and Hidden Active Galactic Nuclei in Star-Forming Galaxies at Redshift ¿0.3, The Astrophysical Journal, 764, 176

- Juneau, S., Dickinson, M., Alexander, D. M., & Salim, S. 2011, A New Diagnostic of Active Galactic Nuclei: Revealing Highly Absorbed Systems at Redshift ¿0.3, The Astrophysical Journal, 736, 104
- Kauffmann, G., Heckman, T. M., & Tremonti, C. 2003, The host galaxies of active galactic nuclei, Monthly Notices of the Royal Astronomical Society, 346, 1055
- Kewley, L., Dopita, M., Sutherland, R. S., Heisler, C. A., & Trevena, J. 2001, Theoretical Modeling of Starburst Galaxies, The Astrophysical Journal, 556, 121
- Kocevski, D. D., Lubin, L. M., Lemaux, B. C., Gal, R. R., Fassnacht, C. D., Lin, R., & Squires, G. K. 2009, Properties Of Galaxies Hosting X-ray-selected Active Galactic Nuclei In The CL1604 Supercluster At z = 0.9, The Astrophysical Journal, 700, 901
- Larson, R. & Tinsley, B. 1978, Star formation rates in normal and peculiar galaxies, The Astrophysical Journal, 219, 46
- Lifshitz, E. M. 1946, On the gravitational stability of the expanding universe, Zhurnal Eksperimentalnoi i Teoreticheskoi Fiziki, 16, 587
- Magorrian, J. & Tremaine, S. 1998, The Demography of massive dark objects in galaxy centers, The Astronomical Journal, 115, 2285
- Martini, P. 2004, Why does low-luminosity AGN fueling remain an unsolved problem?, Proceedings of the International Astronomical Union, 1, 235
- Martini, P., Dicken, D., & Storchi-Bergmann, T. 2013a, The Origin of Dust in Early-Type Galaxies and Implications for Accretion onto Supermassive Black Holes, The Astronomical Journal, 766, 121

- Martini, P. & Kelson, D. 2002, An Unexpectedly High Fraction of Active Galactic Nuclei in Red Cluster Galaxies, The Astrophysical Journal, 576
- Martini, P., Kelson, D., & Kim, E. 2006, Spectroscopic Confirmation of a Large Population of Active Galactic Nuclei in Clusters of Galaxies, The Astronomical Journal, 644, 116
- Martini, P., Miller, E., & Brodwin, M. 2013b, The Cluster And Field Galaxy Active Galactic Nucleus Fraction At Z = 1-1.5: Evidence For A Reversal Of The Local Anticorrelation Between Environment And Agn Fraction, The Astronomical Journal, 768
- Martini, P., Mulchaey, J., & Kelson, D. 2007, The Distribution of Active Galactic Nuclei in Clusters of Galaxies, The Astrophysical Journal, 664, 761
- Martini, P., Regan, M., Mulchaey, J. S., & Pogge, R. W. 2003, Circumnuclear Dust in Nearby Active and Inactive Galaxies. II. Bars, Nuclear Spirals, and the Fueling of Active Galactic Nuclei, The Astrophysical Journal, 589, 774
- Martini, P., Sivakoff, G. R., & Mulchaey, J. S. 2009, The Evolution of Active Galactic
 Nuclei in Clusters of Galaxies To Redshift 1.3, The Astrophysical Journal, 701, 66
 Mo, H., den Bosch, F. V., & White, S. 2010, Galaxy Formation and Evolution, 1st
 edn. (Cambridge University Press), 840
- Orr, M. J. L. & Browne, I. W. A. 1982, Relativistic beaming and quasar statistics, , 200, 1067
- Pierce, C., Lotz, J., & Primack, J. 2010, The Effects of an AGN on Host Galaxy Colour and Morphology Measurements, Monthly Notices of the Royal Astronomical Society, 405, 718

- Pović, M. 2012, AGN-host Galaxy Connection: Morphology and Colours of X-ray selected AGN at z 2., Astronomy & Astrophysics, 541, 23
- Press, W. & Schechter, P. 1974, Formation of galaxies and clusters of galaxies by self-similar gravitational condensation, The Astrophysical Journal, 187, 425
- Rasmussen, J. & Bai, X. 2012, Hot and Cold Galactic Gas in the NGC 2563 Galaxy Group, The Astrophysical Journal, 747, 31
- Richardson, C. & Allen, J. 2014, Interpreting the Ionization Sequence in AGN Emission-line Spectra, Monthly Notices of the Royal Astronomical Society, 437, 2376
- Rovilos, E. & Georgantopoulos, I. 2007, Optical colours of AGN in the extended Chandra deep field South: obscured black holes in early type galaxies, Astronomy & Astrophysics, 475, 115
- Schawinski, K. & Urry, C. 2014, The green valley is a red herring: Galaxy Zoo reveals two evolutionary pathways towards quenching of star formation in early-and late-type galaxies, Monthly Notices of the Royal Astronomical Society, 440, 889
- Shabala, S., Kaviraj, S., & Silk, J. 413, AGN Feedback Drives the Colour Evolution of Local Galaxies, Monthly Notices of the Royal Astronomical Society, 4
- Smoot, G. & Bennett, C. 1992, Structure in the COBE differential microwave radiometer first-year maps, The Astrophysical Journal, 396
- Stern, D., Eisenhardt, P., & Gorjian, V. 2005, Mid-infrared Selection of Active Galaxies, The Astrophysical Journal, 631, 163

- Storchi-Bergmann, T., Simões Lopes, R. D., McGregor, P. J., Riffel, R. A., Beck, T., & Martini, P. 2010, Feeding versus feedback in NGC 4151 probed with Gemini NIFSII. Kinematics, Monthly Notices of the Royal Astronomical Society, 402, 819
- Tomczak, A. R., Tran, K.-V. H., & Saintonge, A. 2011, A Census Of Mid-infrared-selected Active Galactic Nuclei In Massive Galaxy Clusters At 0 Z 1.3, The Astrophysical Journal, 738, 65
- Toomre, A. & Toomre, J. 1972, Galactic bridges and tails, The Astrophysical Journal, 178, 623
- Trump, J., Konidaris, N., & Barro, G. 2013, Testing Diagnostics of Nuclear Activity and Star Formation in Galaxies at z; 1, The Astrophysical Journal, 763
- Vikhlinin, A., Kravtsov, A., Burenin, R., Ebeling, H., Forman, W., Hornstrup, A., Jones, C., Murray, S., Nagai, D., Quintana, H., & Others. 2009, Chandra Cluster Cosmology Project III: Cosmological Parameter Constraints, The Astrophysical Journal, 692, 1060
- Webb, T., O'Donnell, D., & Yee, H. 2013, The Evolution Of Dusty Star Formation In Galaxy Clusters To z = 1: Spitzer IR Observations Of The First Red-sequence Cluster Survey, The Astronomical Journal, 146, 84
- White, M., Martini, P., & Cohn, J. 2008, Constraints on the Correlation Between QSO Luminosity and Host Halo Mass from High-redshift Quasar Clustering, Monthly Notices of the Royal Astronomical Society, 390, 1179
- White, S. & Rees, M. 1978, Core condensation in heavy halos: a two-stage theory for galaxy formation and clustering, Monthly Notices of the Royal Astronomical Society, 183, 341

- Woo, J.-h., Treu, T., Barth, A. J., Wright, S. A., Walsh, J. L., Misty, C., Martini, P., Bennert, V. N., Canalizo, G., Filippenko, A. V., & Gates, E. 2010, The Lick AGN Monitoring Project: The MBH sigma Relation For Reverberation-Mapped Active Galaxies, The Astronomical Journal, 716
- Zeldovich, Y. 1972, A Hypothesis, Unifying the Structure and the Entropy of the Universe, Monthly Notices of the Royal Astronomical Society, 160